AGU PUBLICATIONS

Tectonics

RESEARCH ARTICLE
10.1002/2014TC003730

Neotectonics of the Western Nepal Fault System: Implications for Himalayan strain partitioning

Calvin R. P. Silver[1], Michael A. Murphy[1], Michael H. Taylor[2], John Gosse[3], and Thomas Baltz[1]

[1]Department of Earth and Atmospheric Sciences, University of Houston, Houston, Texas, USA, [2]Department of Geology, University of Kansas, Lawrence, Kansas, USA, [3]Department of Earth Sciences, Dalhousie University, Halifax, Nova Scotia, Canada

Key Points:
- An active fault system has been found in the Dhaulagiri Himalaya
- This fault links with similar regional structures to create the WNFS
- The WNFS is the northeast boundary of a continental fore-arc sliver

Correspondence to:
C. R. P. Silver,
calvin.silver@gmail.com

Citation:
Silver, C. R. P., M. A. Murphy, M. H. Taylor, J. Gosse, and T. Baltz (2015), Neotectonics of the Western Nepal Fault System: Implications for Himalayan strain partitioning, *Tectonics*, *34*, 2494–2513, doi:10.1002/2014TC003730.

Received 8 SEP 2014
Accepted 28 OCT 2015
Accepted article online 3 NOV 2015
Published online 22 DEC 2015

Abstract Oblique convergence at the Himalayan margin is hypothesized to be partitioned by orogen-normal thrusting and orogen-parallel strike-slip faulting. We conducted field mapping and remote sensing in the Dhaulagiri Range of Nepal, and the results reveal an active regional fault system termed the Western Nepal Fault System (WNFS). Right and normally offset Quaternary deposits and brittly deformed bedrock demarcate dextral slip along two strike-slip faults striking N40–50°W linked via an extensional right step over striking N10–20°E. The strike-slip attitudes subparallel bedrock foliation, while the step over cuts at a high angle (~70°). Fault slip data along the strike-slip segments trend N70°W with minor dip component, top to north. Fault slip data and observed kinematics along the WNFS support our interpretation that the WNFS formed via arc-parallel stress. On the basis of geometry, kinematics, and structural position we correlate the WNFS to active faults between the Karakoram and Bari Gad faults. This suggests an ~350 km long dextral fault system extending obliquely across the Western Nepal Himalaya which appears to intersect the Main Frontal Thrust (MFT) near 83°30′E, coinciding with a large gradient in the arc-parallel component of GPS velocities. We interpret the WNFS to represent a class of orogen-parallel strike-slip faults working with subduction to accommodate obliquely convergent plate motion. Our observations support the hypothesis that the region lying between the MFT and the WNFS is a continental version of a fore-arc sliver bounded at its base by the Main Himalayan Thrust.

1. Introduction

Strain within convergent margins around the world is commonly partitioned along first-order structures which accommodate different components of the total strain. Strike-slip faulting coeval with thrusting is common in arcuate convergent margins where the convergence direction is oblique to the plate boundary and interpreted to result from partitioning of the convergence into an orogen-normal and orogen-parallel components [e.g., *Tapponnier and Molnar*, 1979; *Armijo et al.*, 1986, 1989; *Mount and Suppe*, 1987; *Zoback et al.*, 1987; *Ekström and Engdahl*, 1989; *Barrier et al.*, 1991; *Jackson and Molnar*, 1991; *McCaffrey*, 1991, 2009; *Jones and Wesnousky*, 1992; *Molnar*, 1992; *Braun and Beaumont*, 1995; *McCaffrey and Nábelek*, 1998; *Seeber and Pêcher*, 1998; *Glodny et al.*, 2005; *Vernant and Chéry*, 2006; *Styron et al.*, 2011; *Veloza et al.*, 2012; *Murphy et al.*, 2014; *Kundu et al.*, 2014]. While the shape of the original Himalayan margin at the initiation of collision is uncertain, the modern plate boundary is remarkably arcuate in map view between Namche Barwa (eastern Himalayan syntaxis) and Nanga Parbat (western Himalayan syntaxis). The relative motion between India and Eurasia is north-northeastward at a rate of approximately 32 mm yr^{-1} in the western Himalaya and 36 mm yr^{-1} in the eastern Himalaya [*Bettinelli et al.*, 2006]. The arcuate shape coupled with a nearly fixed convergence direction can be used to segment the orogen into three regions: a central sector where convergence is dominantly perpendicular to the orogen and two sectors on the east and west sides where convergent stress is accommodated by partitioning orogen-perpendicular and orogen-parallel components (Figure 1). The chiefly margin-perpendicular compression exhibited from the moment tensors in the central region contrasts with the inclusion of strike-slip moment tensors in the Himalayan wedge west and east of the central region. While intraseismic strain partitioning is difficult to demonstrate in regions with long recurrence intervals, this kinematic framework predicts that fault systems create strain-partitioned regions and non–strain-partitioned regions [*Seeber and Pêcher*, 1998; *Whipp et al.*, 2014].

We present maps and field evidence of a portion of regionally extensive active dextral fault system which we interpret to extend obliquely across the western Himalayan thrust wedge. This system of faults is referred to as the Western Nepal Fault System (WNFS) and is interpreted to delineate the strain-partitioned region in the

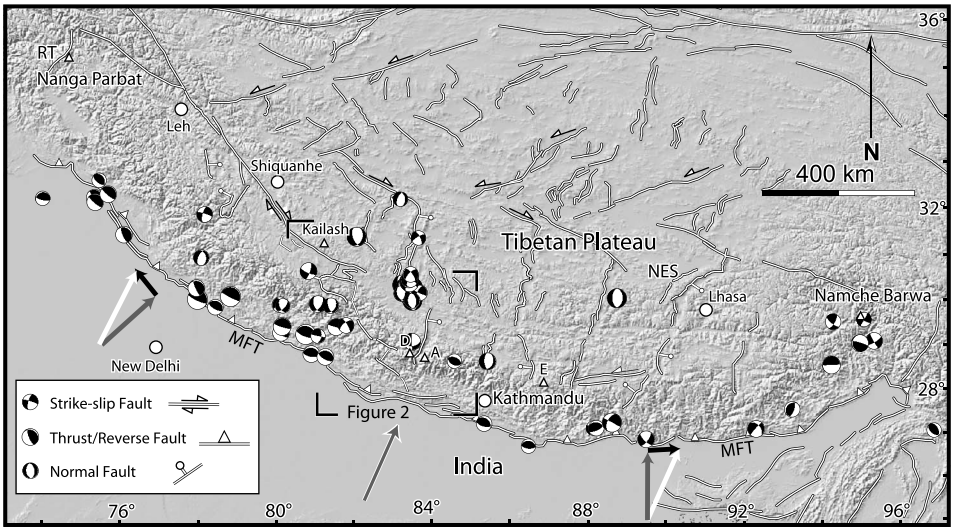

Figure 1. Active faults map of the Tibet Himalayan orogen compiled from *Styron et al.* [2010, 2011] and *Taylor and Yin* [2009]. White arrow shows the azimuth of the motion of India relative to Eurasia calculated by *Bettinelli et al.* [2006]. Black arrow is arc-parallel component. Gray arrow shows arc-normal component. Abbreviations: A = Annapurna; D = Dhaulagiri; E = Everest; MFT = Main Fontal Thrust; NES = Nyainqentangla extensional system; and RT = Raikot thrust. Focal mechanisms are from the Global Centroid Moment Tensor catalogue (1976 to present).

western Himalaya and a non–strain-partitioned region in the central Himalaya [*Murphy et al.*, 2014]. We place the WNFS into a broader context by explaining its role in the 3-D geodynamics predicted in recent modeling by others and predict that a similar albeit more complex system may exist across the eastern Himalaya thrust wedge [*Murphy et al.*, 2014].

2. Active Deformation in the Nepal Himalaya

Structures within the Himalayan thrust wedge absorb as much as 2 cm yr^{-1} of convergence between the Indian Plate and stable Eurasia [*Bilham et al.*, 1997; *Jouanne et al.*, 1999; *Larson et al.*, 1999; *DeCelles et al.*, 2001; *Wang et al.*, 2001; *Chen et al.*, 2004; *Robinson*, 2008; *Ader et al.*, 2012]. The crustal-scale geometry of the Himalaya can be viewed as an arcuate wedge containing large thrust faults that sole into the Main Himalayan Thrust (MHT) at its base [*Gansser*, 1964; *Zhao et al.*, 1993; *Bendick and Bilham*, 2001; *Robinson*, 2008] (Figure 1). In this classic view, the MHT separates the Himalayan wedge from the subducting Indian Plate and breaks the surface in the sub-Himalaya along the Main Frontal Thrust (MFT) [*Pandey et al.*, 1999; *Cattin and Avouac*, 2000; *Lavé et al.*, 2005; *Sapkota et al.*, 2012] (Figure 1). Neotectonic studies along the front of the Himalayan wedge indicate that deformation in the Himalaya is concentrated along the MFT [*Mugnier et al.*, 1999; *Lavé and Avouac*, 2000; *Kumar et al.*, 2006], above a crustal-scale ramp in the MHT located at the base of the High Himalaya in central Nepal [*Molnar*, 1987; *Pandey et al.*, 1999; *Lemmonier et al.*, 1999], as well as in the Shillong Plateau in the eastern Himalaya [*Banerjee et al.*, 2008].

Active internal deformation within the Himalayan wedge has been a focus of much debate, with interpretations ranging from passive translation of the wedge over a basal ramp [*Molnar*, 1987; *Jackson and Bilham*, 1994; *Avouac*, 2003; *Grandin et al.*, 2012], to out-of-sequence thrusting within the wedge in the vicinity of the Main Central Thrust (MCT) [*Wobus et al.*, 2003, 2005], to orogen-normal extension [*Hurtado et al.*, 2001; *McDermott et al.*, 2013]. The former interpretation views the Himalaya as a coherent stable-to-critical thrust wedge with deformation focused at the toe (front) of the wedge, while the latter implies significant internal deformation suggesting that the thrust wedge is in a subcritical state.

Two main structures within the thrust wedge are the MCT and South Tibet Detachment System (STDS). Recent slip along them is interpreted in central Nepal between the Dhaulagiri and Annapurna Himalaya. Cooling histories interpreted from muscovite $^{40}Ar/^{39}Ar$ and apatite fission track thermochronology, and erosion rates interpreted from ^{10}Be concentrations in modern stream sediment, correlate with observed

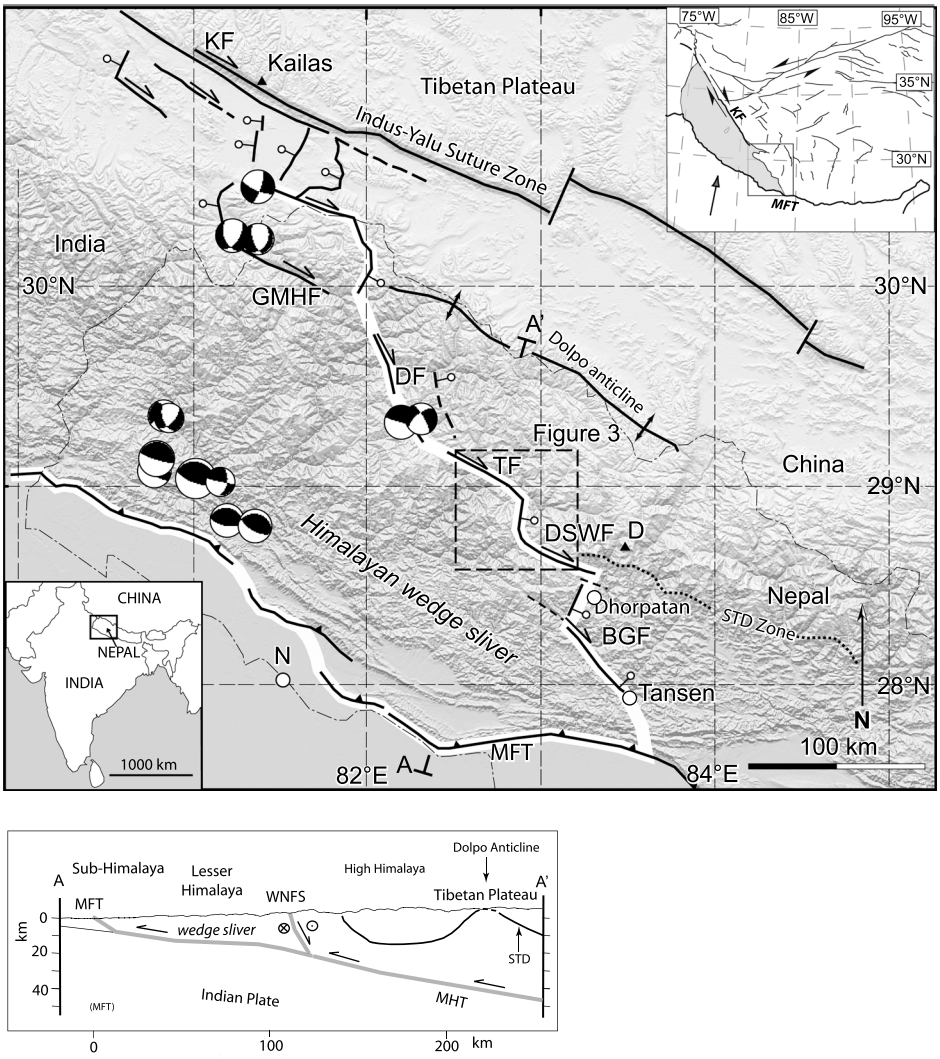

Figure 2. Map of western Nepal showing the system of active dextral faults cutting obliquely across the Himalayan thrust wedge via extensional step overs (modified after *Murphy et al.* [2014]). White line defines the boundary of a hypothesized Himalayan wedge sliver. Inset in the top right corner shows the hypothesized extent of the sliver in gray. Schematic cross section across the thrust wedge highlights the sliver geometry. Abbreviations: MHT = Main Himalayan Thrust; WNFS = Western Nepal Fault System; MFT = Main Frontal Thrust; KF = Karakoram fault; GMH = Gurla Mandhata-Humla fault; DF = Darma fault; TF = Tibrikot fault; DSWF = Dhaulagiri Southwest Fault; BGF = Bari Gad fault; D = Dhaulagiri; and N = Nepalgunj.

steepening of river gradients along the Annapurna front [*Wobus et al.*, 2003, 2005; *Hodges et al.*, 2004; *McDermott et al.*, 2013]. This change straddles mapped segments of the MCT, suggesting slip along the MCT between 4 Ma and present. West of the Annapurna Himalaya, recent slip along the STDS has been interpreted near the southern end of the Thakkhola graben on the south shoulder of Dhaulagiri I. Structural relationships documented by *Hurtado et al.* [2001] suggest that the Dangardzong fault, on the west side of Thakkhola graben, terminates against the Dhumpu detachment within the STDS zone. Discordant alluvium in offset river terraces across the Dangardzong fault was radiocarbon dated at 17.2 ka. The age of these terraces, predating offset, constrains the Dhumpu detachment to have been active within that time.

In addition to thrusting along the MFT, there is evidence of strike-slip faulting in northwest Nepal [*Nakata*, 1989; *Styron et al.*, 2011; *Murphy et al.*, 2014]. A system of right-stepping dextral faults extends from the Mount Kailash region into western Nepal (Figure 2). Faults which have been identified with recent dextral movement include the Karakoram fault, Darma fault, the Tibrikot fault, Dhaulagiri Southwest Fault (DSWF),

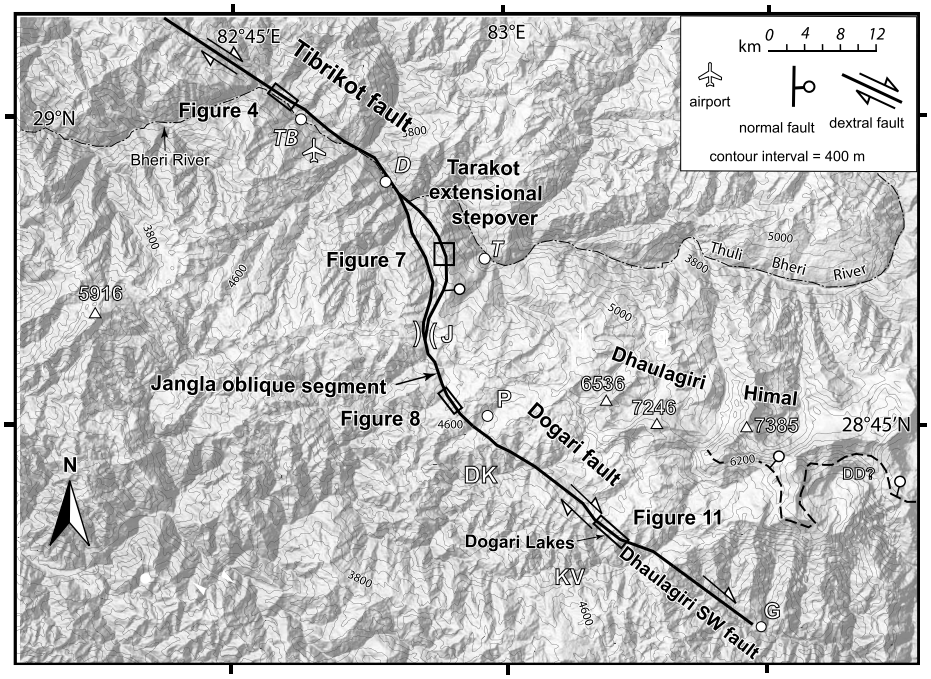

Figure 3. Map showing the WNFS (modified after *Murphy et al.* [2014]). Abbreviations: TB = Tibrikot; D = Dunai; T = Tarakot; J = Jangla Pass; P = Purbang; DK = Dogari Khola; KV = Kape Valley; and DD = Dhaulagiri detachment.

and the Bari Gad fault (BGF) [*Nakata*, 1989; *Murphy and Burgess*, 2006; *Styron et al.*, 2011; *Murphy et al.*, 2014] (Figure 2).

How these dextral faults in the western Himalaya extend across the thrust belt eastward into central Nepal is uncertain. *Hurtado et al.* [2001] suggest a potential connection between the Dhumpu detachment and the Dhaulagiri Southwest Fault, a recently active structure first mapped by *Nakata* [1989] and *Nakata et al.* [1990] in the Dhaulagiri Himalaya. The DSWF was originally mapped as a dextral fault with minor normal dip slip, although *Hurtado et al.* [2001] interpreted the fault to accommodate primarily normal shear. In addition, *McDermott et al.* [2015] mapped a 15–20° north dipping fault, termed the Dhaulagiri detachment in the Dhaulagiri Himalaya STDS zone north of Dhorpatan (Figure 2). The detachment is expressed as a 1–10 m thick brittle-ductile shear zone within the Tethyan Sedimentary Sequence structurally above the interpreted Dhumpu and Annapurna detachments [*Hurtado et al.*, 2001]. Ductile fabrics in this shear zone indicate normal and dextral slips. (U-Th)/He apatite cooling ages indicate cooling of its footwall at $<$3.4 Ma, which is interpreted to reflect exhumation related to slip along the detachment. The Dhaulagiri, Dhumpu, and Annapurna detachments are interpreted to be western extensions of the Machhapuchhare and Phu detachments in the Annapurna Himalaya [*Hurtado et al.*, 2001; *McDermott et al.*, 2015]. The westward continuation of the Dhaulagiri detachment suggests the occurrence of faulting in the western Dhaulagiri Himalaya at $<$3.4 Ma.

Recently, *Murphy et al.* [2014] proposed that the WNFS is part of a regionally extensive active dextral fault system in the High Himalaya of western Nepal. In this contribution we present a comprehensive documentation of the field relationships exposed along the WNFS and discuss its role in the development of the Himalayan thrust wedge.

3. The Western Nepal Fault System

Geologic mapping was conducted on 1:50,000 scale topographic base maps, Advanced Spaceborne Thermal Emission and Reflection Radiometer and Shuttle Radar Topography Mission digital elevation models, and GeoEye-1 satellite images. Our mapping shows that the WNFS can be viewed as consisting of three active fault segments and two northwest striking dextral segments (Tibrikot and Dogari) that are linked via a right-stepping extensional step over (Tarakot to Jangla) (Figure 3).

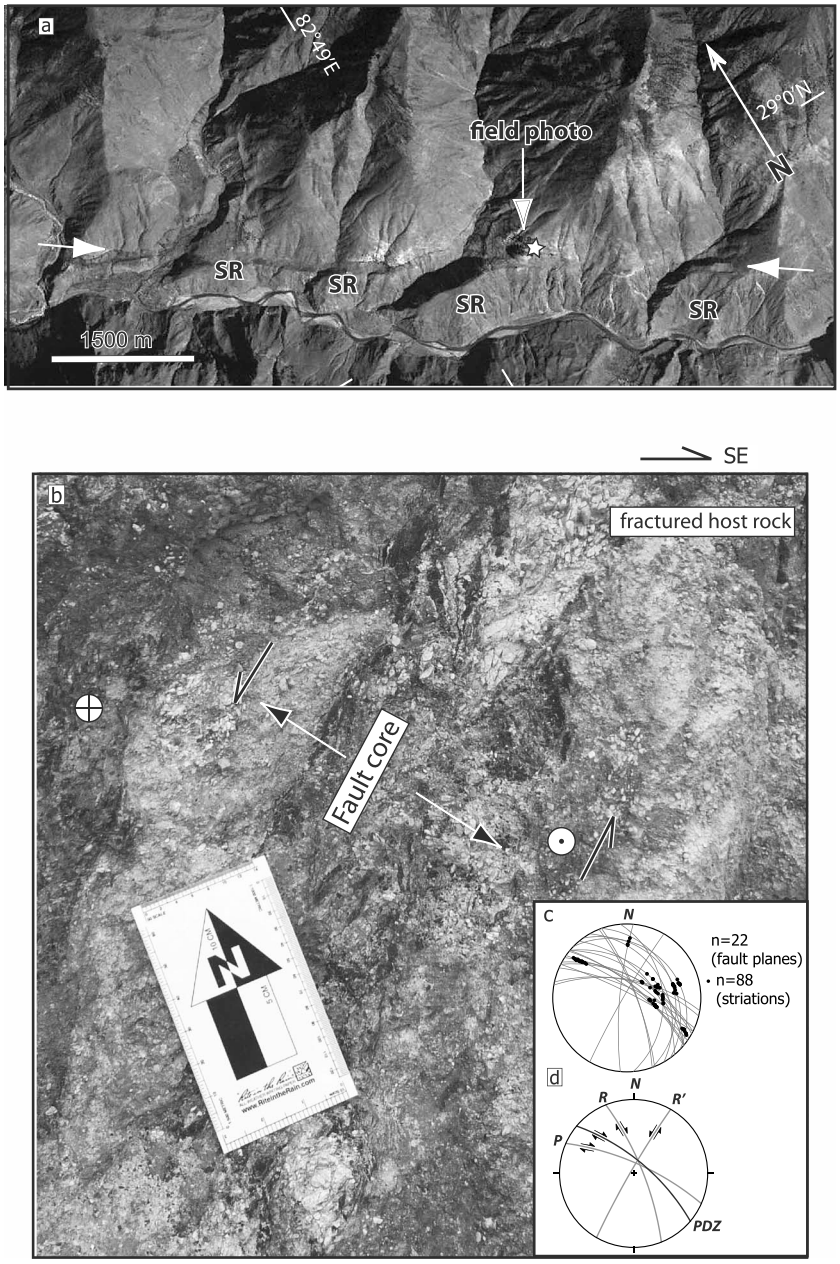

Figure 4. (a) Google Earth image of the Tibrikot fault (TF) showing shutter ridges (SR). (b) Field photo of Tibrikot fault zone. (c and d) Plots of fault slip data. Refer to text for explanation.

3.1. Tibrikot Strike-Slip Segment

The Tibrikot segment is 12 km long and strikes N50–55°W through Lesser and Greater Himalayan rocks. It is well exposed between the villages of Tibrikot (29°1′31.55″N, 82°47′16.33″E) and Suligad (28°52′30.5″N, 82°52′30.5″E) [*Styron et al.*, 2011]. At Tibrikot village the Tibrikot fault zone consists of a monolithologic 2 m wide zone (gray and white quartzite) that contains several 1–3 cm thick fault cores with greenish gray sandy clay gouge. Fault surfaces within the Tibrikot fault zone generally strike NW and dip moderately to steeply toward the NE (Figure 4). Three sets of secondary fault surfaces (fault surfaces truncated by throughgoing fault surfaces) can be distinguished based on their geometry and shear sense with respect to the main trace of the Tibrikot fault (Figure 4). Sets 1–3 strike NNE, NW, and WNW, respectively. All sets dip steeply. The first set displays features indicating left-slip shearing. The second and third sets display features indicating right-slip

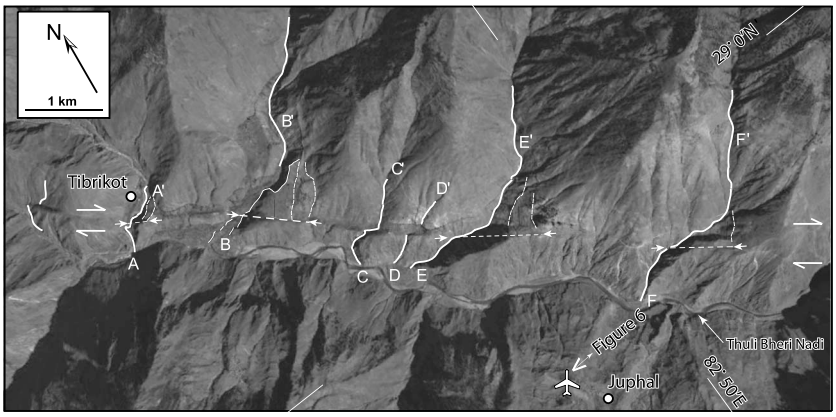

Figure 5. CORONA satellite image of the Tibrikot fault segment showing six primary offset stream channels and shutter ridges. Letters indicate offset downstream (e.g., A) and upstream (e.g., A') channels. Solid white lines are active stream channels, and dashed white lines are truncated terrace risers used in the slip measurement. Slip magnitude is measured using the upstream terrace riser located farthest from the downstream active stream channel. The strike-slip component is denoted by the fault-parallel dashed white lines in between arrows.

shearing. Based on their geometry and shear sense directions, we interpret these secondary fault sets as Riedel shear surfaces associated with right-lateral shear along the Tibrikot fault.

The main strand of the Tibrikot fault truncates and dextrally offsets south flowing streams and associated terraces and fans (Figures 5 and 6). Stream offsets show varying dextral separations along strike of the fault trace. Measurements were calculated on GeoEye satellite images by extrapolating undeformed reaches of streams or offset terraces to the observed fault trace. This methodology was utilized to minimize the effects of near-fault uncertainty generated by channel erosion (differing greatly from channel to channel due to relative stream age and catchment size) and preexisting bedrock structure [*Gold et al.*, 2009]. Measurements are as follows: A: 335 m, B: 818 m, C: 186 m, D: 138 m, E: 841 m, and F: 735 m (Figure 5: from west to east, respectively). Error in this measurement comes from challenges in geomorphic interpretation

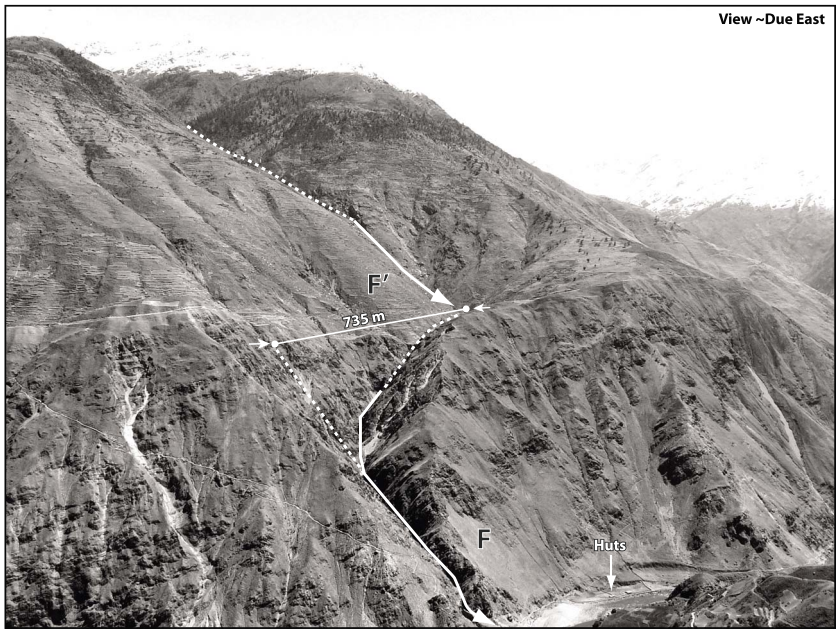

Figure 6. Field photo of one offset drainage along the Tibrikot fault segment. Terraced fields and foot paths are visible along the trace. Offset drainage F-F' is highlighted.

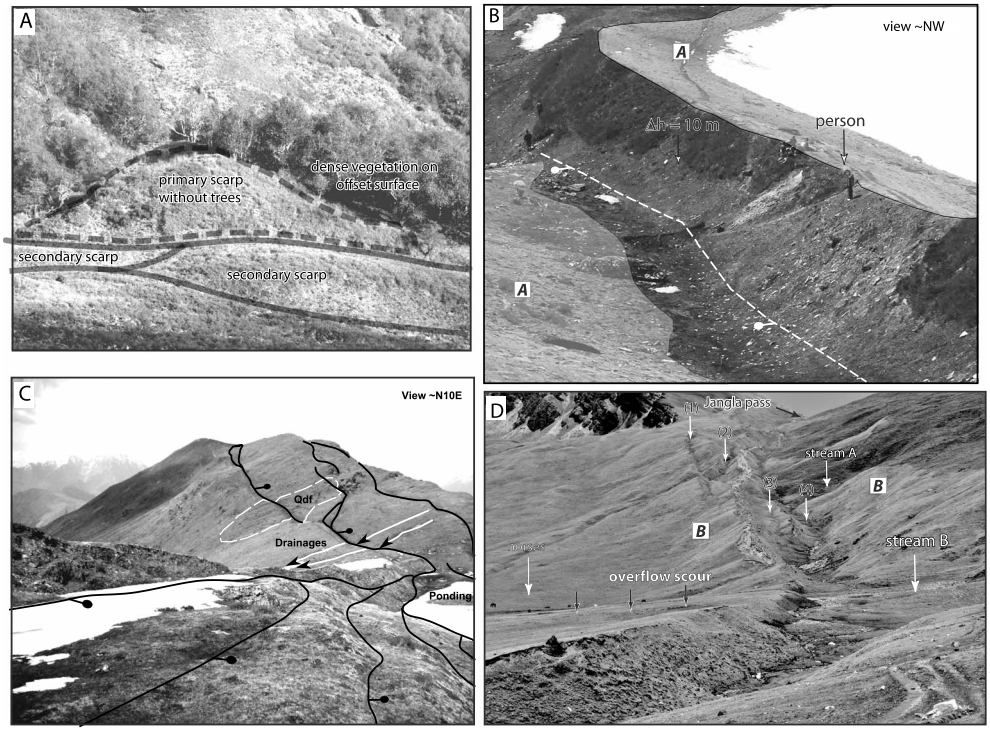

Figure 7. (a) Field photo of scarp faces with limited growth and multiple traces cutting heavily vegetated surfaces southeast of Dunai in Jangla Valley. (b) Field photo of Tarakot extensional step over showing the fault with the largest discrete segment of scarp with its steep fault-controlled face and the cut "A" surface having similar dip and surficial deposits (also shown in *Murphy et al*. [2014]). (c) Field photo of Tarakot extensional step over showing distributed and anastomosing fault traces that cut a Quaternary debris flow and minor drainages with west transport direction; ponding has occurred near one of the larger scarps. (d) Field photo of the Jangla oblique segment south of the Jangla Pass (also shown in *Murphy et al*. [2014]). Erosion in the valley base has generated a fault line scarp. Surface B are cut by fault traces.

and the previously stated effects of channel erosion and bedrock structure controls. Therefore, modern channel positions and widths are utilized as margins of error on each respective stream, assuming this width is tied to an interplay of catchment size, age of incision, and subsequent offset. Channel widths are also measured on GeoEye satellite imagery. Combined with offset measurements, the results are as follows: A: 335 ± 56 m, B: 818 ± 29 m, C: 186 ± 6 m, D: 138 ± 4 m, E: 841 ± 18 m, and F: 735 ± 12 m. The addition of channel widths as error limits is noted as an interpretive methodology. However, it highlights the complexity of the geomorphology at Tibrikot, suggesting a wide range of possible offset distances. To minimize the impact of these uncertainties, which are common to all stream/terrace riser offset constraints for fault slip, we used a multiple stream approach along the reaches of the Tibrikot fault. While each stream offset may have an uncertainty (typically $<$5%), only dextral slip can explain the vast majority of observed offsets, stream morphology, and shutter ridges (Figures 4–6).

3.2. Tarakot Extensional Step Over

The southeast extent of the Tibrikot fault is difficult to discern in satellite imagery due to heavy forest growth and possible river erosion. However, field mapping around Dunai village shows a distributed system of north striking fault scarps that primarily dip to the east. The fault bifurcates near Dunai at the hydroelectric power plant (Figure 3) and reconnects 14 km to the south. The eastern segment strikes along a ridge above Tarakot, while the adjacent western segment strikes up a north-south forested valley that ends at Jangla Pass.

The eastern Tarakot segment appears as traces along the ridge above tree line 12 km southeast of Tibrikot and extends for ~10 km striking N10–20°E, subperpendicular to the Tibrikot strike-slip segment (28°51′6.49″N, 82°57′4.71″E). Along the crest of the ridge, the scarps are anastomosing and distributed over half a kilometer in width (Figure 7c). The scarps cut soils and sediments consisting of a mixture of poorly

sorted colluvial diamicts and moderately sorted stream gravels. Large angular clasts show coarse deep randomly oriented scratches acquired by mass movement, not subglacial flow. In many locations the offset alpine surfaces are capped by several centimeters of postglacial loess growing a wide range of grasses and tundra vegetation with shallow roots (Figures 7b and 7d).

On the Tarakot segment, scarps expose ruptured sediment and bedrock with curvilinear surface traces [*Murphy et al*., 2014]. The primary western fault scarp shows a maximum above ground displacement of 10 m with a prominent displacement gradient along strike (Figure 7b). Numerous splays branch off this primary scarp into distributed zones of strain with as little as 0.2 m of displacement on minor scarps. These smaller scarps also exhibit displacement gradients along strike. In places, scarp height is inversely proportionate with the number of scarps, suggesting a simple strain partitioning over a region of uniform stress. *Murphy et al*. [2014] measured topographic transects across the scarp network to quantify throw and scarp morphology. The scarps in the north and south (e.g., scarps shown in the foreground in Figure 7c) have relatively rounded crests and are generally covered with a fine carpet of grass. Toward the center of the network the scarps have sharper crests and planar faces (Figure 7b). The latter scarps exhibit less vegetation, which reflects instability either because the scarps are simply steeper and more erosive or because they were ruptured more recently.

The highest scarp on the Tarakot segment, 10 m vertically, exhibits a definite bevel at about 3 m from the top. The upper slope is ~30°, and the lower slope is ~40°. Both slopes have a height of ~5 m. There is a clear change from dense shrub growth on the upper slope to little growth on the lower slope, and locally, this change corresponds with the bevel (Figure 7b). All soils exposed in the scarps were inceptisols or gelisols, so soil development was not a significant control on scarp morphology. The beveling seems too sharp and laterally extensive to simply be the result of nonlinear diffusion on the most convex portion of the upper slope. We observed no abrupt change in parent material along strike or downdip of the scarp. As interpreted by *Murphy et al*. [2014], the bevel may reflect two or more scarp-forming events, with the lower steeper slope indicating less time to equilibrate. Radiocarbon dating of scarp-related sediments at this location suggests that they were deposited between 1165 and 1400 A.D. [*Murphy et al*., 2014]. Reconstruction of the offset was used to calculate an extension rate of 9.9 mm yr^{-1} [*Murphy et al*., 2014].

Several Quaternary deposits are either crosscut by or emanate from the scarps. There are debris flows and inactive solifluction lobes oriented subperpendicular to the fault system on a 22° slope into the western Jangla Valley (Figure 7c). These deposits are offset normally with very little to no right separation of the surficial deposits observed. Uphill-facing scarps have truncated water runoff from the sloping ridge and developed small catchments atop the colluvial wedges. These colluvial wedges are still fresh and are not significantly incised, possibly due to sustained periods of below-freezing temperatures and short summers. In addition to the offset Quaternary deposits, brittle deformation was recorded along bedrock cliffs paralleling and within 100 m of the westernmost extent of the Tarakot segment, where near-vertical cataclasites (1 up to 15 cm wide) confirm the orientation and normal sense of shear.

One kilometer to the west (Figure 3), the subparallel extensional system in the adjacent Jangla Valley has similar map view geometry, N10–20°E with east dipping scarps. Significant erosion of the scarps precludes detailed mapping. We interpret the scarps in the valley to be relatively young for several reasons: (i) surfaces cut by the fault traces have thick arboreal growth, while the free faces have minimal shrub growth with no trees (Figure 7a); (ii) the escarpment faces are relatively planar with little diffusive rounding; and (iii) the escarpments exhibit only minor gullying despite their steepness and the high intensity of precipitation during the rainy season.

3.3. Jangla Oblique Segment

Continuing eastward, the western Jangla Valley and eastern Tarakot segments merge near Jangla Pass, 3.5 km to the south (28°49′39.67″N, 82°55′37.63″E) (Figure 9). We define the Jangla oblique segment as the fault trace network between Jangla Pass and Purbang Valley. The Jangla oblique segment strikes approximately N20°W and is characterized by a 0.5 km wide zone of deformation. This network retains a distributed nature but with a more linear trace (Figure 9). Other subparallel traces are observed outside the main deformation zone. The more linear fault segments cut Holocene and older debris flow diamict, alluvial fan gravels, overbank deposits, and loess. The soils are mostly weakly developed (inceptisols). In places the diamict has a

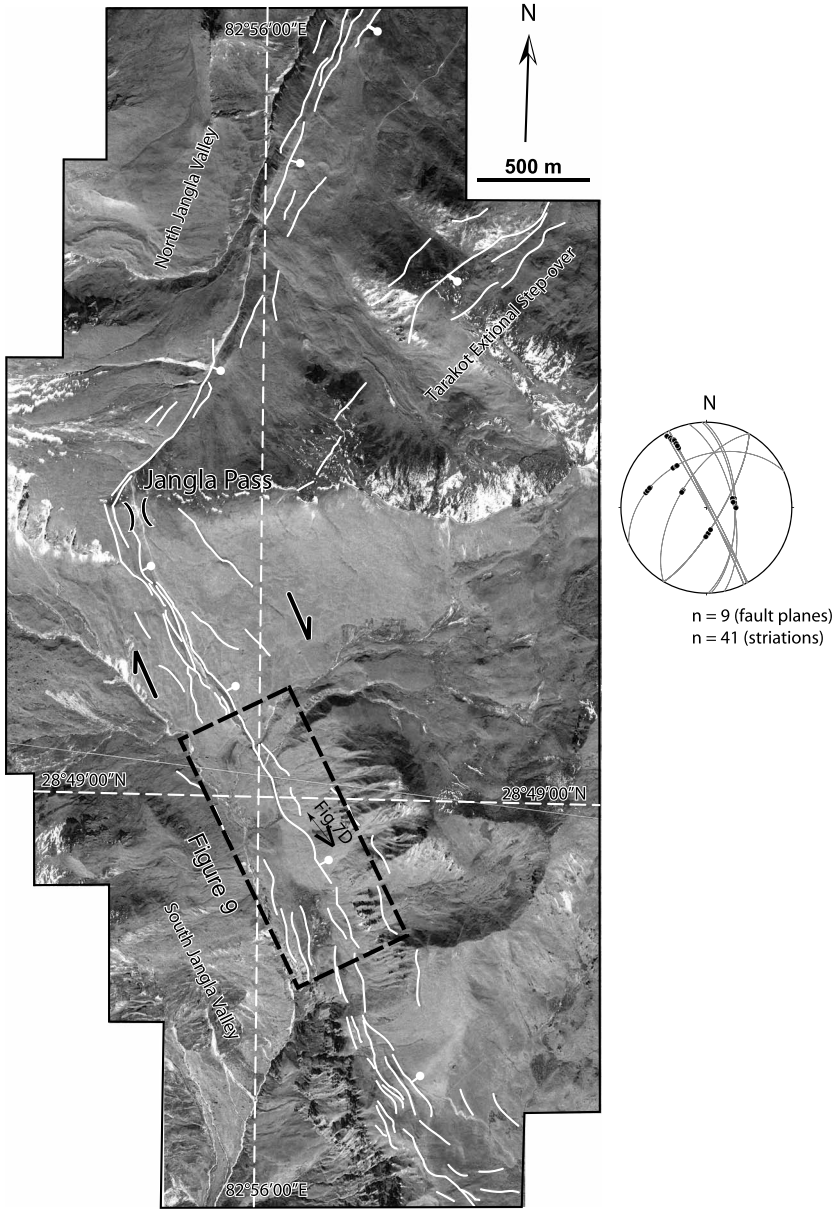

Figure 8. Satellite image of Jangla Pass showing the northern end of the Jangla oblique segment and associated fault slip data. Refer to text for explanation.

slightly better horizonation and greater rubification, but it contains a little more clay than the other parent materials giving the appearance of a strong soil development. On stream terraces, the silty loess and overbank deposits have outsized clasts up to 20 cm long attributed to either flooding or cryoturbation. The lack of soil development (even considering the climate) and the youthful appearance of the landform morphology observed during field work suggest that most of the surfaces are Holocene if not late Holocene.

More than a dozen scarps with sharp crests and planar faces comprise the main segment (Figures 7d and 8). The largest scarps (numbered 1–4 in Figure 7d) have rerouted drainages causing erosion of the colluvial wedges throughout the area. The largest observed scarp (scarp 4 or linked scarps 3 and 4) in the valley is 2.5 m high, but unknown amounts of stream incision at that location seem faster than the erosion of the scarp top, making this value a maximum.

Alluvial fans, debris flows, and drainage systems appear to have been obliquely offset by dextral and normal slip. The largest active fan (Figure 9), sloping perpendicular to the fault scarps, exhibits what is interpreted to

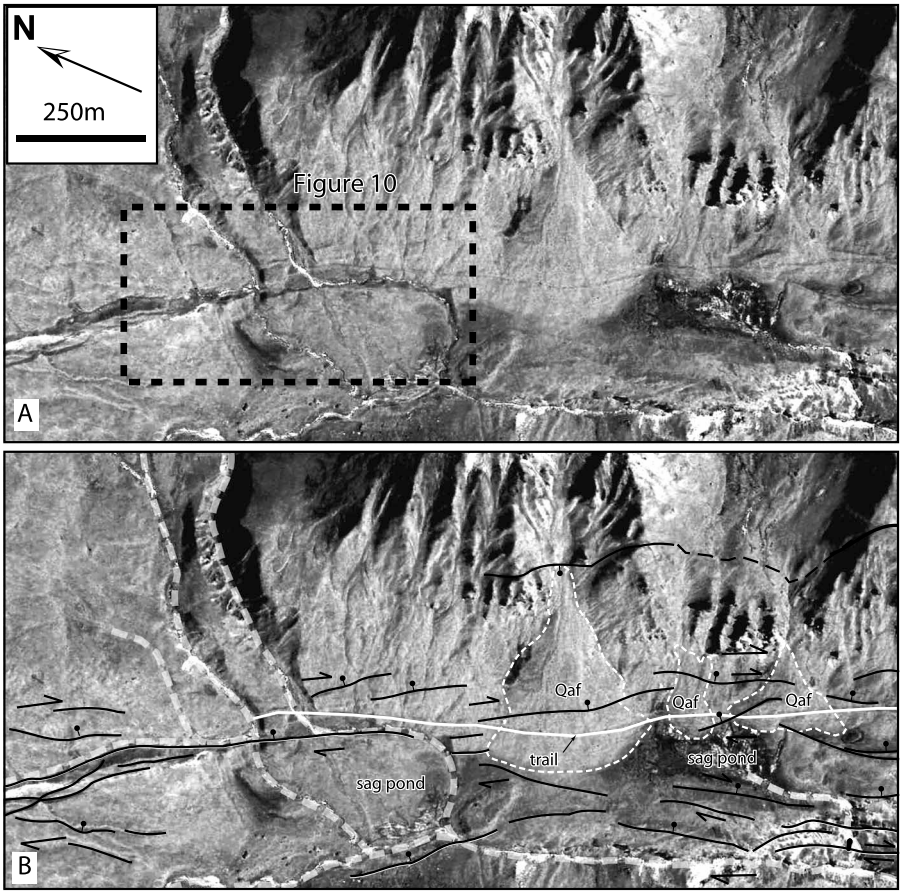

Figure 9. Fault map of a portion of Jangla oblique segment exhibiting the distributed nature of the fault system and the crosscutting relationships with alpine morphology. Quaternary alluvial fans (Qaf; outlined in dashed white lines) and sag ponds are prominent and locally cut by subparallel, east dipping normal faults that show minor right-slip separation. Dashed light gray lines indicate stream channels.

be possible dextral offset based on field observations at its lateral margins and a possible dextral offset of its fan axis. Adjacent to this fan are two smaller fan/debris flow cones which also potentially exhibit dextral offsets. The fans merge with irregular small drainages and are concealed by colluvium, making their offsets difficult to measure precisely and highly interpretive.

Below the pass, at the northern edge of the valley, the primary faults interact with alpine drainages flowing east-northeast to west-southwest (Figure 10a). The consequent streams have incised a Quaternary veneer of debris flows, alluvium, and colluvium on the south facing slope north of the fault. The field correlation of two streams reveals dextral slip. This is corroborated by ponding features, beheaded drainages, and redirected streams.

By correlating the offset terrace risers, we estimate maximum dextral separation of 79 ± 21 m (Figure 10a). Owing mainly to erosion by the migrating streams, the uncertainty in this measurement is based on the width of the incised channels which bound the terrace treads (Figure 10a) [*Gold et al.*, 2009].

A simplified interpretation of how this stream morphology evolved is shown in Figure 10b. Depicted is a two-stream system crossing a dextral strike-slip fault with minor normal offset. The fault has formed or deepened a valley that dips downstream toward the SSE. Figure 10b shows two small drainages, A and B, of subequal width, incising a sloping surface with a dip of 20°. Between the incised valleys resides a tongue-shaped terrace riser which is used for estimating total slip. Initiation of faulting forces dog legging of the streams, causing asymmetrical erosion of the separated terrace risers and increased incision of the west (upthrown, footwall) side (Figure 10b). There is a critical distance of separation between the streams and their hanging wall continuations. Once this critical separation is reached, it is easier for stream A to pond against the fault scarp, subsequently rerouting to channel valley B′. Stream B ponds and moves along the scarp with no other

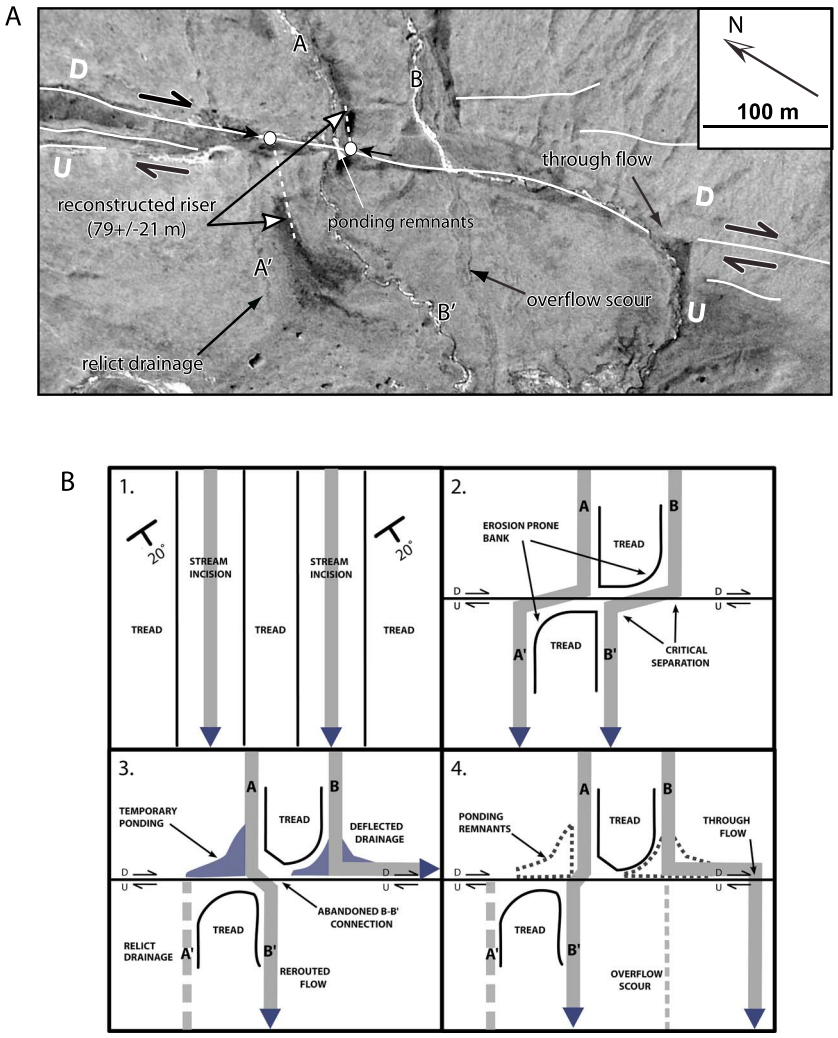

Figure 10. (a) Satellite image shows offset channels and points used to measure the offset river riser (79 ± 21 m) between streams A and B and important geomorphic features to note. Dashed white lines mark the projection of the offset river risers to the fault plane. D = downthrown and U = up thrown. (b) Interpretation of how this system evolved. Interpretation shows two-stream systems offset by an oblique fault. Stage 1: Two streams incising to generate a riser between them on a 20° dipping slope. Stage 2: Oblique motion initiates, and streams A and B are rerouted. Erosion of middle terrace riser begins asymmetrically. Stage 3: At a critical separation ponding occurs as throughflow becomes difficult for both streams. Stream A deviates from A′ and rerouted to B′. Stream B abandons B′, ponding, and flows along the scarp. If the ponding B floods, there will be flow over the scarp. Stage 4: Present-day morphology. Stream A has incised, and ponding no longer occurs. A′ is dry. Overflow scour is seen across the fault from where it has cut through the scarp at a different location.

immediate outlet. Channel A′ is abandoned and becomes a raised and abandoned streambed. The previously linked terrace risers are now separated by a dry streambed which once linked stream B to B′. Note the apparent left separation of stream A-B′ despite the dextral slipping fault at this time. Ponding subsides as incision between A and B′ becomes more conducive to flow. If stream B floods, there will be overflow scouring on the footwall adjacent to its bend along scarp. As flow and slip continues, stream B eventually finds a point of incision along the scarp and generates a new path, exhibiting morphology similar to today. Using the slip rate estimated along the nearby Tarakot segment of 9.9 mm yr^{-1}, [*Murphy et al.*, 2014] suggest that these 79 m offset features are approximately 7980 years old.

Fault slip data were collected from bedrock fault zone outcrops flanking Jangla Valley (Figure 7d). Fault surfaces are smooth and typically display ridges, grooves, and striations in a thin <2 mm thick red and green clay gouge. The data show that the measured faults exhibit strike-slip and dip-slip shear senses. The primary strike-slip component is dextral and trends NNW, subparallel to the mapped fault traces in the valley. E-W

normal dip-slip shear is distributed across fault planes of differing strikes which are suborthogonal to the primary strike-slip fault and subparallel to the Tarakot extensional segment, which we interpret to be secondary shears consistent with dextral motion.

The fault segments merge at Purbang Valley on the southeast edge of the Jangla oblique segment (Figure 3). From Purbang southward the fault scarp is visible at ground level and on satellite imagery as primarily a single fault trace, although two and three faults are seen over short segments. This trace can be followed 15 km into the Dogari block just south of the Dogari Himal and Putha Hiunchuli (7246 m) in the Dhaulagiri Range. Along this segment fault strike changes orientation from N10–30°W to N50°W near Dogari Khola with distinct "V"ing across valleys indicating the fault dips to the NNE. The orientation of this fault, as it enters Dogari, is similar in strike to the Tibrikot segment. Along the south facing piedmont, a dextral sense of shear is evident from offset alluvial fan axes and debris flow levees, both which can be traced on both the footwall and hanging wall but which were insufficiently narrow to provide precise estimates of slip.

3.4. Dogari Strike-Slip Segment

Between Dogari Khola and Dogari lakes the trace is heavily eroded for a ~2 km long stretch. The trace is mappable on the south side of the river flowing through Dogari Khola and crosses the ridge between Dogari Valley and Kape Valley to the east. The fault trace strikes approximately N50°W as it reaches the ridge (28°40′9.13″N, 83°5′19.11″E). Satellite imagery shows several possible bifurcations of the fault. However, strands other than the primary fault were difficult to observe on the ground. Although we interpret traces to continue through this region, they are not well exposed. The fault system is mapped as a single trace from Dogari Khola southward. Further field mapping in the region northeast of the main observed trace is necessary to assess the presence of more subparallel fault strands.

Atop the ridge where the main fault trace is visible above tree line are three subparallel valleys draining northeast to southwest with sharp ridges between them. They are clearly glacially modified owing to the presence of extensive basal-scoured lineations observed along the grassy plain, poorly sorted angular to subrounded boulders with glacial striations on bedrock surfaces, and moraine clasts along the length of the valleys, and the glacial cirques at the apex of each of the valleys. Loess deposits blanket these broad valleys, permitting the growth of fine grasses among the rock debris.

These three valleys are crosscut by the fault, generating a number of Quaternary tectonic geomorphic landforms (Figure 11). The most striking features along the fault scarp are two sag ponds; Pond 1 in the west is 380 m at its widest (i.e., fault-parallel distance) and Pond 2 in the east is 420 m. These ponds developed along the scarp face due to damming of the south flowing drainages. Physical measurements (diving) of pond depths indicate 5–10 m depths in 2011. The third valley has no standing water due to a small incised drainage outlet through the fault scarp. The primary fault scarp cuts obliquely across the bedrock foliation at ~20° (Figure 12a). The primary scarp dips ~50–60° to the NE, steeper than the foliation, and is locally covered with thin ($<$1 m) colluvium.

Along most of this segment, the scarp crest remains sharp with little to no erosion, even in the base of the glacial valley. Secondary scarp faces can be seen only on the high edges of the valley with changes in vegetation (probably more owing to differences in soils instead of time), boulder deposits, and crest erosion. They also exhibit a difference in strike from foliation but have a lower dip. Tertiary scarp faces, of similar strike but steeper dip, are resolvable but difficult to map due to erosion and thick surficial deposits (Figure 12b).

Surfaces separated by the fault trace are correlated on the basis of debris type and offset scouring marks within the valley base. The exposed face of the primary scarp is 31 m at the valley edges and 6 m adjacent to the sag ponds (Figure 12a).

A high water mark was observed 1.5 m above the surface of the eastern pond during field work in early June (Figure 12b). No grasses were present below this high water mark though several loess deposits exist on the now exposed banks. No growth on this highly fertile loess, while it is carpeted by fine grass everywhere else, implies that this high water mark is attained at regular intervals due to insufficient drainage. This suggests that stream incision through the scarp is young and minor, not allowing for rapid drainage. Sustained ponding, low incision in an area that receives regular monsoonal precipitation, sharp scarp crests, and fault-controlled primary scarp faces all suggest recent slip along this fault segment.

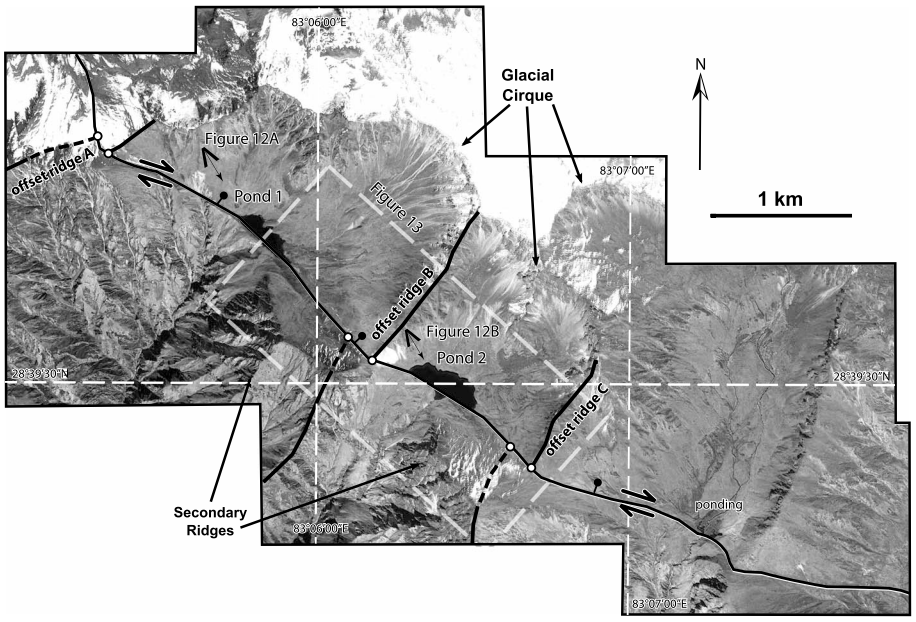

Figure 11. Satellite image of the Dogari segment at the Dogari lakes. Fault displays normal and dextral kinematics. Offset ridges (A–C) between north and south glacially carved valleys. Normal dip separation on the fault trace has generated Pond 1 and Pond 2. Note the extrapolated ridge segments used for slip estimation and piercing points, straight sides of ponds against scarp face, and secondary ridges on protruding wings. The eastern valley does not exhibit the standing water as seen in the other two valleys, nor is its eastern ridge offset.

Minimum dextral separation of the primary ridges bounding the glacial valleys is observed in satellite imagery (Figures 11 and 13). Correlating the ridges is most consistent with dextral offsets (ridges A–C, respectively) at 152 m, 180 m, and 163 m. These values are obtained by extrapolation of the straight ridgelines into the fault trace and palinspastically restoring them along the fault surface (Figure 13). In this extrapolation we disregard the possibility of minor changes in the ridgelines related to surficial processes. By utilizing the minimum and maximum offset values, we estimate an average dextral offset of 165 ± 25 m in the Dogari region from all three ridges.

Additional offset correlations are possible. In the footwall between the two ponding valleys a prominent ridge strikes subparallel to those used for the primary offset correlation above. This ridge is juxtaposed against the glacial valley across the fault, consistent with a shutter ridge geometry (Figure 13). A similar shutter ridge is present on the eastern ridge as well, though the secondary ridge here is less distinct. Restoration of the shutter ridges results in dextral offsets of ~464 m and ~414 m, respectively, 439 ± 25 m based on ridge width (Figure 13). The dip-slip component between the hanging wall and footwall ridge crests is less than 100 m. This suggests that the Dogari segment has primarily accommodated dextral slip with a relatively minor normal component, similar to the Tibrikot fault. The range of strike-slip offsets along the Dogari fault segment agrees within error. However, we attempt to reconcile the observed range in offsets by suggesting processes that would alter the offset magnitudes. The most likely is that fault motion initiated prior to the most recent glaciation. The lateral margins of the offset ridgelines on the south side of the fault show glacial modification.

Surface ruptures caused by normal dip slip would be erased if slip was concurrent with or prior to glaciation in the valleys. The presence of the relatively uneroded 6 m primary scarp in the base of the glacial valley suggests recent postglacial motion (Figure 12a). The timing of glacial events in the Himalaya has been shown to be variable along strike of the range [e.g., *Owen and Dortch*, 2014]. Results from a nearby study at the Gurla Mandhata massif show that the last glacial advance as recorded by moraines at the mouths of most valleys ranges in age between 28 and 64 ka [*Owen et al.*, 2010]. However, the correlation of glacial features between these two localities remains uncertain. To estimate a first-order age approximation for landforms with the largest offsets, we use the 9.9 mm yr^{-1} Tarakot slip rate measurement [*Murphy et al.*, 2014]. The

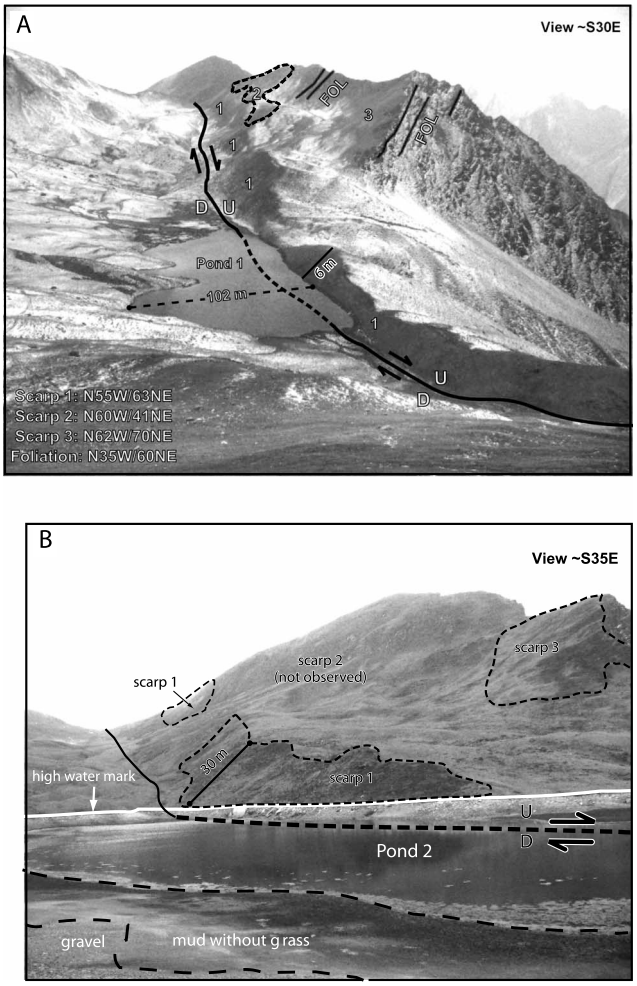

Figure 12. (a) Field photo of Pond 1. Fault trace is at base of scarp faces. 1: primary scarp, 2: secondary scarp, and 3: tertiary scarp, and FOL: foliation layers with 20–25° difference in strike from foliation. Glacial motion is from left to right (north to south). Note the sharp scarp crest and differential height of scarp, higher on the margins of the valley and lower in the middle. (b) Field photo along the shore of Pond 2. High water mark of pond is noted in white. Shore is made up of gravely deposit and tan mud with no growth. Scarps 1 (30 m) and 3 are visible in the background though no scarp 2 is observed in the Pond 2 valley.

conservative measurement of 165 m strike-slip offset via primary ridge reconstruction at Dogari would yield an age of 16,700 years old, while the maximum correlation of ridge offsets of 439 m suggests an age of 44,000 years. We note that the 9.9 mm yr^{-1} slip rate is high compared to that estimated by GPS studies in western Nepal [*Jouanne et al*., 2004] and slightly higher than the 7–8 mm yr^{-1} slip rate determined by *Chevalier et al*. [2012] along the southern Karakoram fault. This rate discrepancy may in part be due to the along-strike evolution of the WNFS. Active faults to the north in southern Tibet are associated with ductile shear zones with large magnitudes of slip that initiated in the Miocene [*McCallister et al*., 2014]. To the south no ductile shear zone that can be correlated with the WNFS has been recognized. Although we only have a partial understanding of the geometry of the fault system between southern Tibet and southern Nepal (Tansen), it appears to consist of several segments which are probably not completely linked, and therefore, this slip rate is unlikely to apply to all fault segments. Thus, these first-order estimates of landform age are highly unconstrained and are the focus of current research efforts.

In summary, the field observations presented above indicate that the WNFS is an active fault system striking approximately N50°W across the Dhaulagiri Himalaya linking the Tibrikot fault to the Dhaulagiri Southwest Fault. Dextral motion is transferred to the southeast from the Tibrikot fault across the north striking Tarakot extensional step over to the approximately N50°W striking Jangla and Dogari segments (Figure 3). Beyond the Dogari lakes the fault trace extends N50°W across Kape Valley to the ridge west of Dhaula Valley (Figure 3). The scarps mapped in Kape Valley are the westernmost extent of the previously recognized Dhaulagiri Southwest Fault [*Nakata*, 1989; *Nakata et al*., 1990]. The Dogari segment is interpreted to link to the DSWF which extends southeast to the village of Gurjagoan (28°35′13″N, 83°14′09″E). We did not map east of this village.

4. Discussion

4.1. Fault or Sackungen?

While in the Tarakot step over segment and Dogari fault zones, we debated [*Murphy et al*., 2014] an alternative interpretation that explains the scarps as sackungen, which formed by gravitational collapse of high topography. Sackungen are scarps generated by massive deep-seated landslides and are common at high elevations in

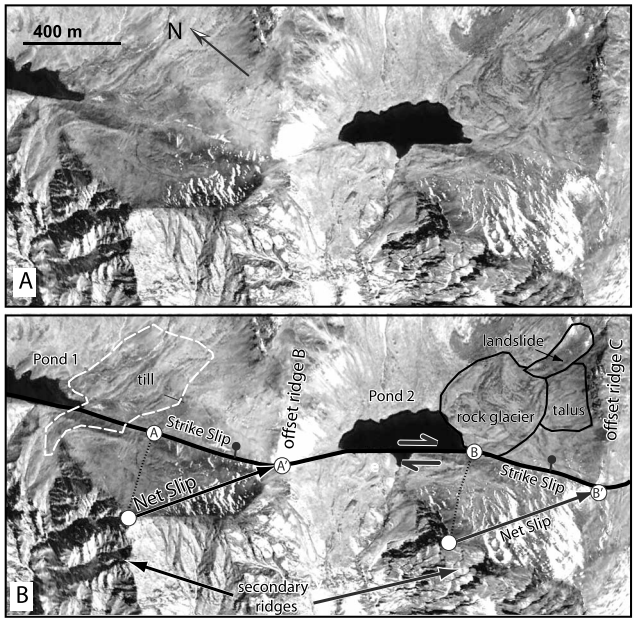

Figure 13. Satellite image of dextral shoulders protruding into the valleys associated with Ponds 1 and 2. Offset of ridges B and C can be interpreted differently by using the secondary ridges for correlation. Piercing points are labeled to denote locations for secondary measurements.

regions of high relief [e.g., *McCalpin and Irvine*, 1995; *Ambrosi and Crosta*, 2006]. They have been reported throughout the Himalayas [*Shroder*, 1998; *Shroder and Bishop*, 1998; *Dunning et al*., 2009]. They commonly, but not always, dip upslope and parallel the bedrock fabric for long distances and can cross topographic ridges. The largest documented sackung in the Western Alps is 7 km long [*Tibaldi et al*., 2004]. Along the >62 km length of the WNFS there is clear horizontal dextral slip with negligible to minor normal slip. Thus, on the basis of fault length and the dominant strike-slip motion, we reject the possibility that most of the WNFS is a gravitational sackung. Further, although most of the short extensional and oblique slip fault segments exhibited upslope-facing scarps, they too exhibit dextral strike-slip offsets and dextral shear sense indicators similar to the prominent Tibrikot and Dogari fault segments. The observation that the 10 m high scarp in Holocene sediment in the Tarakot step over aligns with cataclasite 100 m to the west along the cliff gives further confidence that the scarp is genetically related to a major bedrock structure exhibiting oblique normal brittle deformation. At larger scales of observation, the two prominent dextral fault systems (Tibrikot and Dogari) are in close proximity (10 km) but kinematically require a right step to propagate fault slip. The right step in a dextral system would result in transtensional fault kinematics that would predict normal shear sense along the fault segments observed in Tarakot and Jangla Valleys. Thus, our favored interpretation is that the mapped fault scarps are tectonic in origin.

4.2. Kinematics of the WNFS

The fault slip data indicate that the Tibrikot, Tarakot, and Dogari fault segments facilitate east-west displacement and support the interpretation that they are genetically, not just spatially, linked to each other. The slip direction along the fault system approximately parallels the strike of the Himalayan thrust wedge in western Nepal. *Styron et al*. [2011] analyzed GPS data across the Himalayan thrust wedge and show that the arc-parallel velocity component locally parallels the strike of the Tibrikot fault segment. GPS data from station DLP0 at Juphal airport yield an arc-parallel (N57°W) velocity of 5.71 ± 2.25 mm yr^{-1} [*Styron et al*., 2011]. Our field observations of fault-related landforms are consistent with an arc-parallel velocity that is subparallel to the Tibrikot fault. The Tibrikot fault is thus interpreted to primarily accommodate arc-parallel motion via dextral slip. The right-stepping Tarakot extensional step over is kinematically linked to Tibrikot and in turn also accommodates arc-parallel motion. This supports the observation of Tarakot being a normal fault system with minor dextral slip thereby acting as an extensional step over in a regional dextral fault system.

Due to linkage of the Tarakot extensional step over to the Jangla oblique segment, it seems reasonable to assume that it also accommodates arc-parallel motion. More convincing evidence for recent dextral motions along this fault segment is based on the field observations and offset reconstructions of faulted landforms consistent with approximately 79 m of right slip.

The variation of slip magnitude from between 138 and 841 m of dextral slip at the Tibrikot fault to 165 and 439 m dextral slip at Dogari suggests that arc-parallel motion is propagating toward the southeast. The difference in slip magnitude across the WNFS indicates a decrease in arc-parallel motion from west to east along the fault system. An increase in dip-slip activity is locally observed which may correlate to an increase

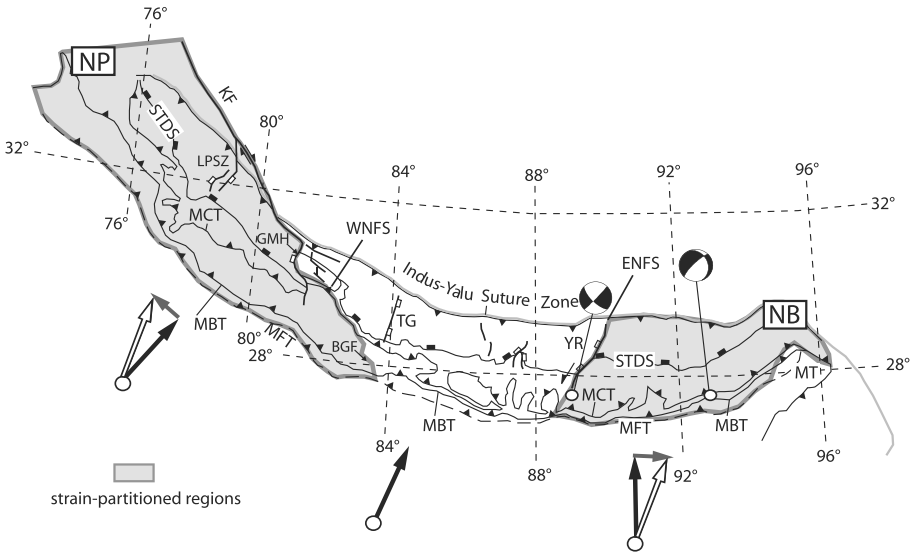

Figure 14. Map of the Himalayan arc showing strain-partitioned regions in the west and east resulting from oblique convergence. Open arrow shows the azimuth of the motion of India relative to Eurasia calculated by *Bettinelli et al.* [2006]. Gray arrow is arc-parallel component. Black arrow shows arc-normal component. NP = Nanga Parbat; KF = Karakoram fault; STDS = South Tibet Detachment System; LPSZ = Leo Pargil Shear Zone; MCT = Main Central Thrust; GMH = Gurla Mandhata-Humla fault; MBT = Main Boundary Thrust; MFT = Main Frontal Thrust; WNFS = Western Nepal Fault System; ENFS = Eastern Nepal Shear Zone; BGF = Bari Gad fault; TG = Thakkhola graben; YR = Yadong rift; and NB = Namche Barwa.

in arc-normal stress near the southern extent of the WNFS in the central Himalaya and may provide an explanation for recent arc-normal extension along the Dhaulagiri detachment and its incorporation into the arc-parallel extensional regime [*McDermott et al.*, 2013, 2015]. The difference in slip magnitude also arises from the likely age difference of offset features as well as the manner in which the fault system evolved. The fault system may have simply propagated from the northwest near the GMH fault to the Bari Gad fault segment in the southeast or to the Dhaulagiri detachment fault in the east. More likely, the fault system evolved as a set of isolated faults that eventually linked as they grew longer and interconnected. Future geochronological information for the offset features will bear directly on this outstanding question.

4.3. Regional Extent of the WNFS

The NW projection of the WNFS extends to dextral faults in southwestern Tibet that include the Karakoram fault and Gurla Mandhata-Humla fault [*Nakata*, 1989; *Murphy et al.*, 2002; *Murphy and Copeland*, 2005; *Murphy and Burgess*, 2006; *Chevalier et al.*, 2012] (Figure 1). These faults extend southeastward via north striking extensional right step overs which include the Gurla Mandhata detachment [*McCallister et al.*, 2014; *Chevalier et al.*, 2012], Tackche fault, and Darma fault (Figure 14). Although their recent slip history is not thoroughly documented, they all appear to cut Quaternary landforms and display morphologies consistent with active faulting. The SE projection of the WNFS beyond this study's field area extends toward dextral faults that include the Dhaulagiri southwest and Bari Gad faults [*Nakata*, 1989; *Yeats et al.*, 1992] (Figure 1). This fault linkage requires the presence of a structure linking the WNFS to the Bari Gad fault. We speculate that this hypothesized structure extends NNW from the NW end of the Bari Gad fault along the west side of Dhorpatan village (28°29′N, 83°02′E).

This NW striking dextral fault system obliquely cuts across the width of the Himalayan thrust wedge. Its location may relate to other observations: (1) the WNFS coincides with a NW trending belt of seismicity [*Pandey et al.*, 1999; *Cattin and Avouac*, 2000] and (2) it parallels a NW trending dislocation in simulations of the interseismic velocity field with a locking depth at 21–17 km (approximate local depth of the MHT) and is affected by 19 mm yr^{-1} of thrusting and 0–7 mm yr^{-1} of dextral slip [*Larson et al.*, 1999; *Jouanne et al.*, 1999, 2004]. The dextral slip rate by *Murphy et al.* [2014] is a rate determined over two seismic cycles and is slightly higher than the maximum value of the interseismic geodetic rate. Collectively, these faults and supporting geophysical data suggest a >350 km long zone of active dextral shear cutting obliquely across the Himalayan thrust

wedge forming a branch line with the MFT near Tansen (Figure 2). Our interpretation that the Karakoram fault is kinematically linked to the WNFS deviates from previous interpretations that have the Karakoram fault extend eastward along the India-Asia suture zone [e.g., *Lacassin et al*., 2004] and facilitates eastward extrusion of southern Tibet. Our interpretation that active slip on the Karakoram fault is fed into the Himalayan thrust wedge implies that right slip along the India-Asia suture zone ceased, and by extension, eastward extrusion of southern Tibet by the time the WNFS initiated. This is supported by geologic mapping in south central Tibet (~84°30′E) which shows little to no strike-slip faulting along the suture zone [*Murphy et al*., 2010].

4.4. Himalayan Sliver

The WNFS accommodates dextral slip and a lesser amount of extension. The position of the WNFS is at a place along the arcuate-shaped Himalayan orogen where the convergence direction is oblique to the plate boundary. Based on the geometry, kinematics, and position of the WNFS in the thrust wedge, we interpret that it belongs to a class of orogen-parallel strike-slip faults that work in concert with subduction to accommodate obliquely convergent plate motion. This interpretation implies that the region lying between the MFT and the WNFS is a continental version of a fore-arc sliver [e.g., *Fitch*, 1972; *Platt*, 2000] bounded at its base by the MHT. This region of the thrust wedge is referred to as the Himalayan sliver which is actively being translated WNW (with respect to the Indian Plate), parallel to the strike of the Himalayan arc (Figure 2) [*Murphy et al*., 2014]. The WNFS forms the eastern boundary of the Himalayan sliver. We imagine that the western boundary of the sliver is composed of a diffuse system of shortening structures in the northern Pamir Mountains [*Robinson*, 2009] and in the Nanga Parbat region as proposed by *Seeber and Pêcher* [1998]. Here these structures accommodate NNW-SSE shortening [*Wang et al*., 2001]. The interpretation of a Himalayan sliver implies that it is rigid. This cannot be entirely accurate since it is cut by several active faults, some of which are interpreted to link to ductile shear zones, such as the Leo Pargil and Qusum detachments [*Ni and Barazangi*, 1985; *Hintersberger et al*., 2010; *Saylor et al*., 2010]. Moreover, *Kundu et al*. [2014] suggest that the Himalayan sliver is segmented into two parts in the vicinity of the Kaurik Chango rift based GPS results. The geodynamics of the translation of the sliver is modeled by *Whipp et al*. [2014]. Their arcuate convergence experiment shows that the flux of material into the Nanga Parbat massif needed to sustain high topography and erosion rates can be explained in a 3-D geodynamical model of oblique convergence where strain in the orogenic wedge is partitioned. The flux of material into Nanga Parbat comes from northwestward translation of the Himalayan orogenic wedge. Strain within the Nanga Parbat massif is envisioned to be dominated by vertical motion along faults along its western margin, such as the Raikot thrust fault. This is supported by recent GPS results [*Jouanne et al*., 2014]. The interpretation that the WNFS segments the orogen helps explain the persistence of orogen-normal extensional faulting east of the WNFS [e.g., *Hodges et al*., 2004; *McDermott et al*., 2015] and orogen-parallel extensional faults to the west [*Murphy et al*., 2002]. The zone of right-lateral shear associated with the WNFS may be narrow (~50 km). A recent study by *Cannon and Murphy* [2014] suggests that the region immediately north of the WNFS in the Dolpo and Mugu districts of Nepal is undergoing active uplift due to movement on deep-seated east-west striking shortening structures. However, along strike to the west several studies show that active deformation is characterized by east-west extension [*Chevalier et al*., 2012; *Murphy et al*., 2009]. The juxtaposition of these contrasting structural styles can be explained by segmentation of the Himalayan thrust wedge by the WNFS which separates these kinematic domains. A lack of strain partitioning east of the WNFS in southern Tibet is consistent with geodetic results which suggest that India-Asia convergence is almost entirely absorbed by shortening in the thrust wedge [*Kundu et al*., 2014]. The kinematic model proposed by [*Murphy et al*., 2014] explains the observed WNW oriented extension at the southeast projection of the WNFS near the MFT [*Yeats et al*., 1992]. Here the strike of the Bari Gad fault rotates from WNW to NNW as it approaches the MFT. The fault is mapped as an east dipping normal fault near the village of Tansen (83°30′E). This structural relationship is strikingly similar to that observed in the Sunda Strait where slip along the central Sumatra fault is interpreted to link to extensional structures that strike nearly orthogonal to the Java trench [*Sieh and Natawidjaja*, 2000] and facilitate NW translation of the southwestern Sumatra block [*Huchon and Le Pichon*, 1984]. A similar kinematic relationship is interpreted along the northern Andes of Colombia and Ecuador. There, the Guayaquil-Algeciras right-slip fault system cuts obliquely across the Andes and intersects the subduction plate boundary at the extensional Gulf of Guayaquil forming a partitioned system of strike-slip and normal structures to accommodate oblique convergence between the South American and Nazca Plates [*Veloza et al*., 2012].

4.5. Himalayan Strain Partitioning

If oblique convergence is a first-order control on active deformation in the thrust wedge, then the arc-shaped thrust wedge could be viewed as consisting of a non–strain-partitioned region in the central Nepal Himalaya that is bordered on its west and east sides by strain-partitioned regions (Figure 14). As described above we think that the WNFS is the structure separating the western strain-partitioned region from the non–strain-partitioned region. If valid, this predicts a counterpart to the WNFS in the eastern Himalaya, namely, the Eastern Nepal Fault System (ENFS). We further hypothesize that the strain will be primarily sinistral with minor transtensional left step overs. We suggest that this hypothesized fault system lies along the southwest projection of the Yadong rift, intersecting the MFT at around 88°30′E (Figure 14). The Nyainqentanglha extensional system (Figure 1) is presently strain partitioned by a dominant normal fault and more minor left slip [*Armijo et al*., 1986; *Kapp et al*., 2005]. However, an exhumed strike-slip shear zone is observed in the footwall documenting an earlier history of significant slip partitioning [*Armijo et al*., 1986; *Kapp et al*., 2005]. Kinematically, the ENFS would define the western margin of a sliver of the thrust wedge that is translated eastward. The eastern margin of this sliver could be the NNE striking Mishmi thrust located due south of Namche Barwa (eastern Himalayan syntaxis) [*Thingbaijam et al*., 2008; *Burgess et al*., 2012].

5. Conclusions

The primary results of this study are as follows:

1. Two strike-slip segments are linked by an extensional step over in the high Dhaulagiri Himalaya, herein referred to as the Western Nepal Fault System.
2. Fault scarp morphology, geomorphology, and Quaternary offsets suggest that segments of the fault are active since the last glacial advance.
3. A decrease in dextral slip is observed from NW to SE across the fault's extent.
4. This recent fault system can be correlated with strike-slip structures in NW Nepal to the central Himalaya, thus suggesting a regionally extensive right-slip system.
5. We interpret that the role of this fault is to accommodate the dextral component of oblique convergence in the western Himalaya.
6. Based on examples of strain-partitioned oblique margins worldwide, we note that such a structure is expected.
7. We interpret that this system would serve as the eastern boundary of a "fore-arc" sliver. This sliver is bounded at the southern margin by the MFT and the MHT at its base. We interpret the WNFS as the western half of a first-order symmetric fixture of the strain that results from oblique convergence in an arcuate orogen.

Acknowledgments

We thank Marie-Luce Chevalier and an anonymous reviewer for providing reviews that greatly improved the manuscript. The authors also thank Dave Whipp and Chris Beaumont for their contribution to the development of the fore-arc sliver portion of this paper and Bhim Chand at Earth's Paradise Treks, Expeditions, and Geologistics for his superb logistical support. This research was funded by the University of Houston GEAR program and the General Research Fund from the University of Kansas. Tabulated data can be requested via the first author.

References

Ader, T., et al. (2012), Convergence rate across the Nepal Himalaya and interseismic coupling on the Main Himalayan Thrust: Implications for seismic hazard, *J. Geophys. Res.*, *117*, B04403, doi:10.1029/2011JB009071.

Ambrosi, C., and C. B. Crosta (2006), Large sackung along major tectonic features in the Central Italian Alps, *Eng. Geol.*, *83.1*, 183–200.

Armijo, R., P. Tapponnier, and T. Han (1986), Late Cenozoic right-lateral strike-slip faulting in southern Tibet, *J. Geophys. Res.*, *94*, 2787–2838, doi:10.1029/JB094iB03p02787.

Armijo, R., P. Tapponnier, J. L. Mercier, and T. Han (1989), Quaternary extension in southern Tibet: Field observations and tectonic implications, *J. Geophys. Res.*, *91*, 13,803–13,872, doi:10.1029/JB091iB14p13803.

Avouac, J. P. (2003), Mountain building, erosion, and the seismic cycle in the Nepal Himalaya, *Adv. Geophys.*, *46*, 1–80.

Banerjee, P., R. Bürgmann, B. Nagarajan, and E. Apel (2008), Intraplate deformation of the Indian subcontinent, *Geophys. Res. Lett.*, *35*, L18301, doi:10.1029/2008GL035468.

Barrier, E., P. Huchon, and M. Aurelio (1991), Philippine Fault: A key for Philippine kinematics, *Geology*, *19*, 32–35.

Bendick, R., and R. Bilham (2001), How perfect is the Himalayan arc?, *Geology*, *29*, 791–794.

Bettinelli, P., J.-P. Avouac, M. Flouzat, F. Jouanne, L. Bollinger, P. Willis, and G. R. Chitrakar (2006), Plate motion of India and interseismic strain in the Nepal Himalaya from GPS and DORIS measurements, *J. Geod.*, *80*, 567–589, doi:10.1007/s00190-006-0030-3.

Bilham, R., K. Larson, J. Freymueller, and Project Idylhim (1997), GPS measurements of present-day convergence across the Nepal Himalaya, *Nature*, *386*, 61–64.

Braun, J., and C. Beaumont (1995), Three-dimensional numerical experiments of strain partitioning at oblique plate boundaries: Implications for contrasting tectonic styles in the Southern Coast Ranges, California, and Central South Island, New Zealand, *J. Geophys. Res.*, *100*, 18,059–18,074, doi:10.1029/95JB01683.

Burgess, P., A. Yin, C. S. Dubey, Z. Shen, and T. K. Kelley (2012), Holocene shortening across the Main Frontal Thrust zone in the eastern Himalaya, *Earth Planet. Sci. Lett.*, *357–358*, 152–167.

Cannon, J. M., and M. A. Murphy (2014), Active lower crustal strain and Himalayan seismic hazard revealed by stream channels and regional geology, *Tectonophysics*, *633*(1), 34–42, doi:10.1016/j.tecto.2014.06.031.

Cattin, R., and J. P. Avouac (2000), Modeling mountain building and the seismic cycle in the Himalaya of Nepal, *J. Geophys. Res.*, *105*, 13,389–13,407, doi:10.1029/2000JB900032.

Chen, Q., J. T. Freymueller, Z. Yang, C. Xu, W. Jiang, Q. Wang, and J. Liu (2004), Spatially variable extension in southern Tibet based on GPS measurements, *J. Geophys. Res.*, *109*, B09401, doi:10.1029/2002JB002350.
Chevalier, M.-L., P. Tapponnier, J. Van der Woerd, F. J. Ryerson, R. C. Finkel, and H. Li (2012), Spatially constant slip rate along the southern segment of the Karakorum fault since 200ka, *Tectonophysics*, *530–531*, 152–179.
DeCelles, P. G., D. M. Robinson, J. Quade, P. Copeland, and B. N. Upreti (2001), Stratigraphy, structure, and tectonic evolution of the Himalayan fold-thrust belt in western Nepal, *Tectonics*, *20*, 487–509, doi:10.1029/2000TC001226.
Dunning, S. A., C. I. Massey, and N. J. Rosser (2009), Structural and geomorphological features of landslides in the Bhutan Himalaya derived from Terrestrial Laser Scanning, *Geomorphology*, *103*, 17–29.
Ekström, G., and P. Engdahl (1989), Seismic strain rates in regions of distributed continental deformation, *J. Geophys. Res.*, *94*, 10,231–10,257, doi:10.1029/JB094iB08p10231.
Fitch, T. J. (1972), Plate convergence, transcurrent faults and internal deformation adjacent to Southeast Asia and the western Pacific, *J. Geophys. Res.*, *77*, 4432–4460, doi:10.1029/JB077i023p04432.
Gansser, A. (1964), *The Geology of the Himalayas*, Wiley Interscience, New York.
Glodny, J., J. Lohrmann, H. Echtler, K. Gräfe, W. Seifert, S. Collao, and O. Figueroa (2005), Internal dynamics of the paleoaccretionary wedge: Insights from combine isotope tectonochronology and sandbox modeling of the South-Central Chilean fore-arc, *Earth Planet. Sci. Lett.*, *231*, 23–29.
Gold, R. D., E. Cowgill, J. R. Arrowsmith, J. Gosse, X. Chen, and X. F. Wang (2009), Riser diachroneity, lateral erosion, and uncertainty in rates of strike-slip faulting: A case study from Tuzidun along the Altyn Tagh Fault, NW China, *J. Geophys. Res.*, *114*, B04401, doi:10.1029/2008JB005913.
Grandin, R., M.-P. Doin, L. Bollinger, B. Pinel-Puysségur, G. Ducret, R. Jolivet, and S. N. Sapkota (2012), Long-term growth of the Himalaya inferred from interseismic InSAR measurement, *Geology*, *40*, 1059–1062.
Hintersberger, E., R. C. Thiede, M. R. Strecker, and B. R. Hacker (2010), East-west extension in the NW Himalaya, *Geol. Soc. Am. Bull.*, *122*, 1499–1515.
Hodges, K. V., C. Wobus, K. Ruhl, T. Schildgen, and K. Whipple (2004), Quaternary deformation, river steepening, and heavy precipitation at the front of the Higher Himalayan ranges, *Earth Planet. Sci. Lett.*, *220*, 379–389.
Huchon, P., and X. Le Pichon (1984), Sunda Strait and central Sumatra fault, *Geology*, *12*, 668–672.
Hurtado, J. M., K. V. Hodges, and K. X. Whipple (2001), Neotectonics of the Thakkhola graben and implications for recent activity on the South Tibetan fault system in the central Nepal Himalaya, *Geol. Soc. Am. Bull.*, *113*, 222–240.
Jackson, J., and P. Molnar (1991), Active faulting and block rotations in the Western Traverse Ranges, California, *J. Geophys. Res.*, *96*, 22,073–22,087, doi:10.1029/JB095iB13p22073.
Jackson, M. E., and R. Bilham (1994), 1991–1992 GPS measurements across the Nepal Himalaya, *Geophys. Res. Lett.*, *21*, 1169–1172, doi:10.1029/94GL00917.
Jones, C. H., and S. G. Wesnousky (1992), Variations in strength and slip rate along the San Andreas Fault System, *Science*, *256*, 83–86.
Jouanne, F., J. L. Mugnier, M. R. Pandey, J. F. Gamond, P. LeFort, L. Serrurier, C. Vigny, and J. P. Avouac (1999), Oblique convergence in the Himalayas of western Nepal deduced from preliminary results of GPS measurements, *Geophys. Res. Lett.*, *26*, 1933–1936, doi:10.1029/1999GL900416.
Jouanne, F., J. L. Mugnier, J. F. Gamond, P. Le Fort, M. R. Pandy, L. Bollinger, M. Flouzat, and J. P. Avouac (2004), Current shortening across the Himalayas of Nepal, *Geophys. J. Int.*, *157*, 1–14.
Jouanne, F., A. Awan, A. Pêcher, A. Kauser, J. L. Mugnier, I. Khan, N. A. Khan, and J. Van Melle (2014), Present-day deformation of northern Pakistan from Salt Ranges to Karakorum Ranges, *J. Geophys. Res. Solid Earth*, *119*, 2487–2503, doi:10.1002/2013JB010776.
Kapp, J., T. M. Harrison, P. Kapp, M. Grove, O. M. Lovera, and D. Lin (2005), Nyainqentanghla Shan: A window into the tectonic, thermal, and geochemical evolution of the Lhasa block, southern Tibet, *J. Geophys. Res.*, *110*, B08413, doi:10.1029/2004JB003330.
Kumar, S., S. G. Wesnousky, T. K. Rockwell, R. W. Briggs, V. C. Thakur, and R. Jayangondaperumal (2006), Paleoseismic evidence of great surface rupture earthquakes along the Indian Himalaya, *J. Geophys. Res.*, *111*, B03304, doi:10.1029/2004JB003309.
Kundu, B., R. K. Yadav, B. S. Bali, S. Chowdhury, and V. K. Gahalaut (2014), Oblique convergence and slip partitioning in the NW Himalaya: Implications from GPS measurements, *Tectonics*, *33*, 2013–2024, doi:10.1002/2014TC003633.
Lacassin, R., F. Valli, N. Arnaud, P. H. Leloup, J. L. Paquette, H. Li, P. Tapponier, and M. L. Chevalier (2004), Large-scale geometry, offset, and kinematic evolution of the Karakorum fault, Tibet, *Earth Planet. Sci. Lett.*, *219*, 255–269.
Larson, K., R. Burgmann, R. Bilham, and J. T. Freymueller (1999), Kinematics of the India-Eurasia collision zone from GPS measurements, *J. Geophys. Res.*, *104*, 1077–1093, doi:10.1029/1998JB900043.
Lavé, J., and J. P. Avouac (2000), Active folding of fluvial terraces across the Siwaliks Hills, Himalayas of central Nepal, *J. Geophys. Res.*, *105*(B3), 5735–5770, doi:10.1029/1999JB900292.
Lavé, J., D. Yule, S. Sapkota, K. Basant, C. Madden, M. Attal, and R. Pandey (2005), Evidence for a great Medieval earthquake (~1100 AD) in the central Himalayas, Nepal, *Science*, *307*, 1302–1305.
Lemonnier, C., et al. (1999), Electrical structure of the Himalaya of central Nepal: High conductivity around the mid-crustal ramp along the MHT, *Geophys. Res. Lett.*, *26.21*, 3261–3264.
McCaffrey, R. (1991), Slip vectors and stretching of the Sumatran fore arc, *Geology*, *19*, 881–884.
McCaffrey, R. (2009), The tectonic framework of the Sumatran subduction zone, *Annu. Rev. Earth Planet. Sci.*, *37*, 345–366.
McCaffrey, R., and J. Nábelek (1998), Role of oblique convergence in the active deformation of the Himalayas and southern Tibet plateau, *Geology*, *26*, 691–694.
McCallister, A. T., M. H. Taylor, M. A. Murphy, R. H. Styron, and D. F. Stockli (2014), Thermochronologic constraints on the late Cenozoic exhumation history of the Gurla Mandhata metamorphic core complex, Southwestern Tibet, *Tectonics*, *33*, 27–52, doi:10.1002/2013TC003302.
McCalpin, J. P., and J. R. Irvine (1995), Sackungen at the Aspen Highlands ski area, Pitkin County, Colorado, *Environ. Eng. Geosci.*, *1.3*, 277–290.
McDermott, J., K. X. Whipple, K. Hodges, and M. van Soest (2013), Evidence for Plio-Pleistocene north–south extension at the southern margin of the Tibetan Plateau, Nyalam region, *Tectonics*, *32*, 317–333, doi:10.1002/tect.20018.
McDermott, J., K. Hodges, K. X. Whipple, M. van Soest, and J. M. Hurtado (2015), Evidence for Pleistocene low-angle normal faulting in the Annapurna-Dhaulagiri region, Nepal, *J. Geol.*, *123*(2), 133–151, doi:10.1086/681219.
Molnar, P. (1987), Inversion of profiles of uplift rates for the geometry of dip-slip faults at depth, with examples from the Alps and the Himalaya, *Ann. Geophys.*, *6*, 663–670.
Molnar, P. (1992), Mountain building—Crust in mantle overdrive, *Nature*, *358*, 105–106.
Mount, V. S., and J. Suppe (1987), State of stress near the San Andreas Fault: Implications for wrenching tectonics, *Geology*, *15*, 1143–1146.

Mugnier, J. L., P. Letutmy, G. Mascle, P. Huyghe, E. Chalaron, G. Vidal, L. Husson, and B. Delcaillau (1999), The Siwaliks of western Nepal: I. Geometry and kinematics, *J. Asian Earth Sci.*, *17*, 629–642.
Murphy, M. A., and W. P. Burgess (2006), Geometry, kinematics, and landscape characteristics of an active transtension zone, Karakoram fault system, Southwest Tibet, *J. Struct. Geol.*, *28*, 268–283.
Murphy, M. A., and P. Copeland (2005), Transtensional deformation in the central Himalaya and its role in accommodating growth of the Himalaya orogeny, *Tectonics*, *24*, TC4012, doi:10.1029/2004TC001659.
Murphy, M. A., A. Yin, P. Kapp, T. M. Harrison, C. E. Manning, F. J. Ryerson, D. Lin, and G. Jinghui (2002), Structural evolution of the Gurla Mandhata detachment system, southwest Tibet: Implications for the eastward extent of the Karakoram fault system, *Geol. Soc. Am. Bull.*, *114*, 428–447.
Murphy, M. A., J. E. Saylor, and D. Ling (2009), Landscape evolution of southwest Tibet based on integrated paleoelevation reconstructions and structural history, *Earth Planet. Sci. Lett.*, *282*, 1–9.
Murphy, M. A., V. Sanchez, and M. Taylor (2010), Syncollisional extension along the India–Asia suture zone, south-central Tibet: Implications for crustal deformation of Tibet, *Earth Planet. Sci. Lett.*, *290*, 233–243.
Murphy, M. A., M. H. T. Taylor, J. Gosse, C. R. P. Silver, D. M. Whipp, and C. Beaumont (2014), Limit of strain partitioning in the Himalaya marked by large earthquakes in western Nepal, *Nat. Geosci.*, *7*, 38–42.
Nakata, T. (1989), Active faults of the Himalaya and India and Nepal, *Geol. Soc. Am. Spec. Publ.*, *232*, 243–264.
Nakata, T., K. Otsuki, and S. H. Khan (1990), Active faults, stress-field, and plate motion along the Indo-Eurasian plate boundary, *Tectonophysics*, *181*, 83–95.
Ni, J., and M. Barazangi (1985), Active tectonics of the western Tethyan Himalaya above the underthrusting Indian Plate: The upper Sutlej River Basin as a pull-apart basin structure, *Tectonophysics*, *112*, 277–295.
Owen, L. A., and J. M. Dortch (2014), Nature and timing of Quaternary glaciation in the Himalayan-Tibetan orogen, *Quat. Sci. Rev.*, *88*, 14–54.
Owen, L. A., Y. Chaolu, R. C. Finkel, and N. K. Davis (2010), Quaternary glaciation of Gurla Mandhata (Naimon'anyi), *Quat. Sci. Rev.*, *29*, 1817–1830.
Pandey, M. R., R. P. Tandukar, J. P. Avouac, J. Vergne, and T. Heritier (1999), Seismotectonics of the Nepal Himalaya from a local seismic network, *J. Asian Earth Sci.*, *17*(5–6), 703–712.
Platt, J. P. (2000), Calibrating the bulk rheology of active obliquely convergent thrust belts and forearc wedges from surface profiles and velocity distributions, *Tectonics*, *19*, 529–548, doi:10.1029/1999TC001121.
Robinson, A. C. (2009), Evidence against Quaternary slip on the northern Karakorum Fault suggests kinematic reorganization at the western end of the Himalayan-Tibetan orogen, *Earth Planet. Sci. Lett.*, *286*, 158–170.
Robinson, D. M. (2008), Forward modeling the kinematic sequence of the central Himalayan thrust belt, western Nepal, *Geosphere*, *4*, 785–801.
Sapkota, S. N., P. Tapponnier, L. Bollinger, K. Klinger, I. Siwakoti, and D. R. Tiwari (2012), Hunting of past earthquake along the Main Frontal Thrust using recent geomorphic feature in the area between Mahara Khola to Dharan in central and eastern Nepal The 27th Himalaya-Karakoram-Tibet Workshop (HKT), 2012, 164.
Saylor, J., P. DeCelles, G. Gehrels, M. A. Murphy, R. Zhang, and P. Kapp (2010), Basin formation in the High Himalaya by arc-parallel extension and tectonic damming: Zhada basin, southwest Tibet, *Tectonics*, *29*, TC1004, doi:10.1029/2008TC002390.
Seeber, L., and A. Pêcher (1998), Strain partitioning along the Himalayan arc and the Nanga Parbat antiform, *Geology*, *26*, 791–794.
Shroder, J. F. (1998), Slope failure and denudation in the western Himalaya, *Geomorphology*, *26*, 81–105.
Shroder, J. F., and M. P. Bishop (1998), Mass movement in the Himalaya: New insights and research directions, *Geomorphology*, *26*, 13–35.
Sieh, K., and D. Natawidjaja (2000), Neotectonics of the Sumatran fault, Indonesia, *J. Geophys. Res.*, *105*, 28,295–28,326, doi:10.1029/2000JB900120.
Styron, R., M. Taylor, and K. Okoronkwo (2010), Database of active structures from the Indo-Asian collision, *Eos Trans. AGU*, *91*(20), 181–182, doi:10.1029/2010EO200001.
Styron, R., M. Taylor, and M. Murphy (2011), Oblique convergence, arc parallel extension, and strike-slip faulting in the High Himalaya, *Geosphere*, *7*, 1–15.
Tapponnier, P., and P. Molnar (1979), Active faulting and Cenozoic tectonics of the Tien Shan, Mongolia, and Baykal regions, *J. Geophys. Res.*, *84*, 3425–3459, doi:10.1029/JB084IB07P03425.
Taylor, M. H., and A. Yin (2009), Active structures in the Himalayan-Tibetan orogen and their relationships to earthquake distribution, contemporary strain field, and Cenozoic volcanism: Implications of stain volcanism, *Geopshere*, *5*(3), 199–214.
Thingbaijam, K. K. S., S. K. Nath, A. Yadav, A. Raj, M. Y. Walling, and W. K. Mohanty (2008), Recent seismicity in northeast India and its adjoining region, *J. Seismol.*, *12*, 107–123.
Tibaldi, A., A. Rovida, and C. Corazzato (2004), A giant deep-seated slope deformation in the Italian Alps studied by paleoseismological and morphometric techniques, *Geomorphology*, *58.1*, 27–47.
Veloza, G., R. Styron, M. Taylor, and A. Mora (2012), Open-source archive of active faults for northwest South America, *GSA Today*, *22*(10), 4–10, doi:10.1130/GSAT-G156A.1.
Vernant, P., and J. Chéry (2006), Mechanical modeling of oblique convergence in the Zagros, Iran, *Geophys. J. Int.*, *165*, 991–1002.
Wang, Q., et al. (2001), Present-day crustal deformation in China constrained by Global Positioning System measurements, *Science*, *294*, 574–577.
Whipp, D. M., C. Beaumont, and J. Braun (2014), Feeding the "aneurysm": Orogen-parallel mass transport into Nanga Parbat and the western Himalayan syntaxis, *J. Geophys. Res. Solid Earth*, *119*, doi:10.1002/2013JB010929.
Wobus, C. W., K. V. Hodges, and K. X. Whipple (2003), Has focused denudation sustained active thrusting at the Himalayan topographic front?, *Geology*, *31*, 861–864.
Wobus, C., A. Heimsath, K. Whipple, and K. Hodges (2005), Active out-of-sequence thrust faulting in the central Nepalese Himalaya, *Nature*, *434*, 1008–1011.
Yeats, R. S., T. Nakata, A. Farah, M. Fort, M. A. Mirza, M. R. Pandey, and R. S. Stein (1992), The Himalayan frontal system, *Ann. Tecton.*, *6*, 85–98.
Zhao, W., K. D. Nelson, and project INDEPTH Team (1993), Deep seismic-reflection evidence for continental underthrusting beneath southern Tibet, *Nature*, *366*, 557–559.
Zoback, M. D., et al. (1987), New evidence on the state of stress of the San Andreas Fault system, *Science*, *238*, 1105–1111.